Phase-Change Slippery Liquid-Infused Porous Surfaces with Thermo-Responsive Wetting and Shedding States

Phase-change Slippery Liquid-infused Porous Surfaces with Thermo-responsive Wetting and Shedding States

Raza Gulfam,[†] Daniel Orejon,[‡,‖] Chang-Hwan Choi,[§] Peng Zhang, [†,*]

[†]Institute of Refrigeration and Cryogenics, Shanghai Jiao Tong University, Shanghai 200240, China

[‡]Institute for Multiscale Thermofluids, School of Engineering, The University of Edinburgh, Edinburgh EH9 3FD, Scotland, U.K

[‖]International Institute for Carbon-Neutral Energy Research (WPI-I^{2}CNER), Kyushu University, 744 Motooka, Nishi-ku, Fukuoka 819-0395, Japan

[§]Department of Mechanical Engineering, Stevens Institute of Technology, Castle Point on Hudson, Hoboken, NJ 07030, USA

ABSTRACT

Slippery liquid-infused porous surfaces (SLIPSs) prepared with phase invariant materials (e.g., Krytox GPL oil) have been increasingly researched as low adhesion engineered functional surfaces in the last decade. However, phase change materials (PCMs) have been scarcely adopted, although they are potential candidates due to their inherent lubricant characteristics as well as temperature-dependent phases empowering unique thermo-responsive switchable wettability. Here, paraffin wax (an organic PCM) has been applied on hydrophobized nanoporous copper substrate to realize the phase-change SLIPSs (PC-SLIPSs) fabricated via spin-coating followed by thermal annealing, which overcomes earlier limitations encountered on the PC-SLIPSs. Advantages of these PC-SLIPSs are: the prompting of a low adhesion Wenzel (LAW) state opposed to earlier completely-pinned Wenzel state in the solid phase, and the optimized slippery state without excess of PCM in the liquid phase. Further, in order to characterize the intimate interactions between liquid

droplets and the different phases of the PC-SLIPSs, i.e., solid, mush, and liquid phases, the contact line dynamics have been comprehensively investigated, unveiling the water droplet adhesion and depinning phenomenon as the function of thermo-responsive wetting states. Lastly, the PC-SLIPSs have also been tested for water vapor condensation, demonstrating the feasibility of dropwise condensation and the shift of droplet size distribution in both the solid and liquid phases. The results suggest that such engineered surfaces have great potential to prompt and tune dropwise condensation via thermo-responsive switchable wettability for heat transfer and water harvesting applications.

Keywords: Slippery liquid-infused porous surfaces; Phase change materials; Paraffin wax; Thermo-responsive wettability; Droplet pinning; Dropwise condensation.

INTRODUCTION

Surface engineering has continuously evolved through the recent decades, assisting to tailor the inherent properties of pristine solid surfaces with superior features.[1,2] Especially, roughness and topography of the structured solid surfaces affect their wettability and droplet mobility significantly. On one hand, a liquid droplet may wet the surface structures partially (e.g., contacting the top region only with air entrapped in the valleys between structures) adopting the Cassie-Baxter state,[3] in which droplets show low pinning with sliding angles as small as 0-10°, enabling efficient droplet mobility. On the other hand, a liquid droplet may wet the surface structures up to different extents, adopting the Wenzel state,[3] hindering the droplet mobility. In addition, depending on the extent of droplet pinning, droplet mobility can also be realized even in the Wenzel state. For weak pinning, a droplet may show a certain mobility at sliding angles of 10-50°,[4] which is henceforth referred to as the low adhesion Wenzel (LAW) state, and for strong pinning, a droplet may show relatively low mobility requiring higher sliding angles of 50-90°,[5] henceforth referred to as the high adhesion Wenzel

(HAW) state. Influenced by the wetting state and droplet adhesion, the contact line dynamics as well as the droplet mobility vary significantly.[6-8]

Novel micro- and nano-fabrication techniques (such as lithography, chemical etching, reactive ion etching and plasma oxidation) allow the design of a wide variety of engineered features on pristine solid surfaces, including random porous network,[9] regular individual deep pores,[10] nano-flowers,[11] nano-pins,[12] nano-wires,[13] honeycomb-based geometries,[14] pillar-on-pore-like geometries,[15] and so forth. By infusing lubricant-based liquids within the micro- and/or nano-structures, liquid-infused surfaces (LISs)[16,17] or slippery liquid-infused porous surfaces (SLIPSs)[18,19] are fabricated with distinct characteristics, such as UV-responsiveness guided pathways,[20] efficient dropwise condensation,[21] fog and water harvesting,[22] anti-icing and anti-frost,[23,24] as well as self-cleaning,[25] etc. However, the stability of lubricants on the SLIPSs/LISs needs further attention.[26] Furthermore, slippery liquids can be categorized in two kinds. One is phase invariant materials such as fluorinated lubricants and silicone oils. The other is phase change materials (PCMs), such as organic waxes (e.g., paraffin wax),[27] animal waxes (e.g., beeswax),[28] plant oils (e.g., peanut oil),[29] thermotropic lubricant[30] and polymers (e.g., PNI-PAAm),[31] resulting in phase-change slippery liquid-infused porous surfaces (PC-SLIPSs). They are highly advantageous ensuring multifunctional properties, encompassing thermo-responsive wettability and anti-icing/frosting features,[29,32] water adhesion,[33] tunable opaqueness,[34] smart control of anisotropic motion of liquid droplets in microreactors as well as in tubes,[35] tunable wettability on guided tracks,[36] liquid adhesion control,[37] and intelligent motion control actuators.[38] Generally, the mechanism of the PC-SLIPSs is governed by the thermo-responsive (temperature-driven) wetting states,[39] leading to switchable wettability across the melting temperature of the PCMs employed. However, it should also be noted that only a few PCMs have the required water-repelling lubricant characteristics essential to realize the PC-SLIPSs.[40]

In the previous investigations on the PC-SLIPSs, two major drawbacks were commonly highlighted. First, the infused PCM induces the completely pinned Wenzel state in the solid phase, resulting in droplet immobility.[32-35] Second, when the solid phase of the PCM switches into the liquid phase, the surface becomes slippery with an excess of liquid film where the water droplet tends to sink.[32-34,36] Both noted drawbacks (i.e., solid phase immobility and water droplets sinking within liquid phase) may limit the applicability of the PC-SLIPSs. Hence, in the present work, we develop and demonstrate an optimal impregnation procedure followed by thermal annealing, which eventually decreases the droplet adhesion of the PC-SLIPSs in the solid phase prompting the low adhesion Wenzel (LAW) state. Moreover, the excess of PCM in the liquid phase inducing a slippery state is also minimized. We employ a chemically oxidized copper substrate, consisting of black-velvety cupric oxide nanoporous structures, to realize the as-presented PC-SLIPSs. Structured copper substrate is hydrophobized[9] and infused with paraffin wax (PCM in this study) via two different impregnating methods: dip coating and spin coating followed by the subsequent thermal annealing for further optimization of the amount of paraffin wax. The surface roughness of the PC-SLIPSs is measured at ambient temperature with a non-contact optical profiler (ZETA 20). The surface morphology of the PC-SLIPSs is further characterized with optical microscopy (OLYMPUS BX51M) at various temperatures covering different phases of paraffin wax, while surface wettability at various temperatures is also assessed via optical contact angle goniometer (OCA-20). In addition, the contact line dynamics is investigated during sessile droplet evaporation at various temperatures. Further, leveraged by the unique LAW state in the solid phase and slippery state in the liquid phase, water vapor condensation tests are conducted. The occurrence of dropwise condensation in both the solid and liquid phases coupled with nucleation density and the remarkable shift of the droplet size distribution depending on the phase of the PC-SLIPSs, is demonstrated for the first time.

RESULTS and DISCUSSION

Fabrication and Characterization of the PC-SLIPSs. The methodology to prepare the PC-SLIPSs is summarized in Figure 1. It includes (Figure 1 from left to right) chemical oxidation of a thin copper plate (0.4 mm in thickness) at 70 °C, washing of the oxidized copper plate with distilled water, its high-temperature baking (180 °C) to ensure formation of cupric oxide nanostructures providing average surface roughness (R_a) of 1.79 µm, cooling at ambient temperature (25 °C), perfluorooctyltriethoxysilane (POTS) coating on nanoporous copper plate to impart hydrophobic characteristics, medium-temperature baking (120 °C) for thermal stabilization of POTS and impregnation with the paraffin wax via dip coating and spin coating.

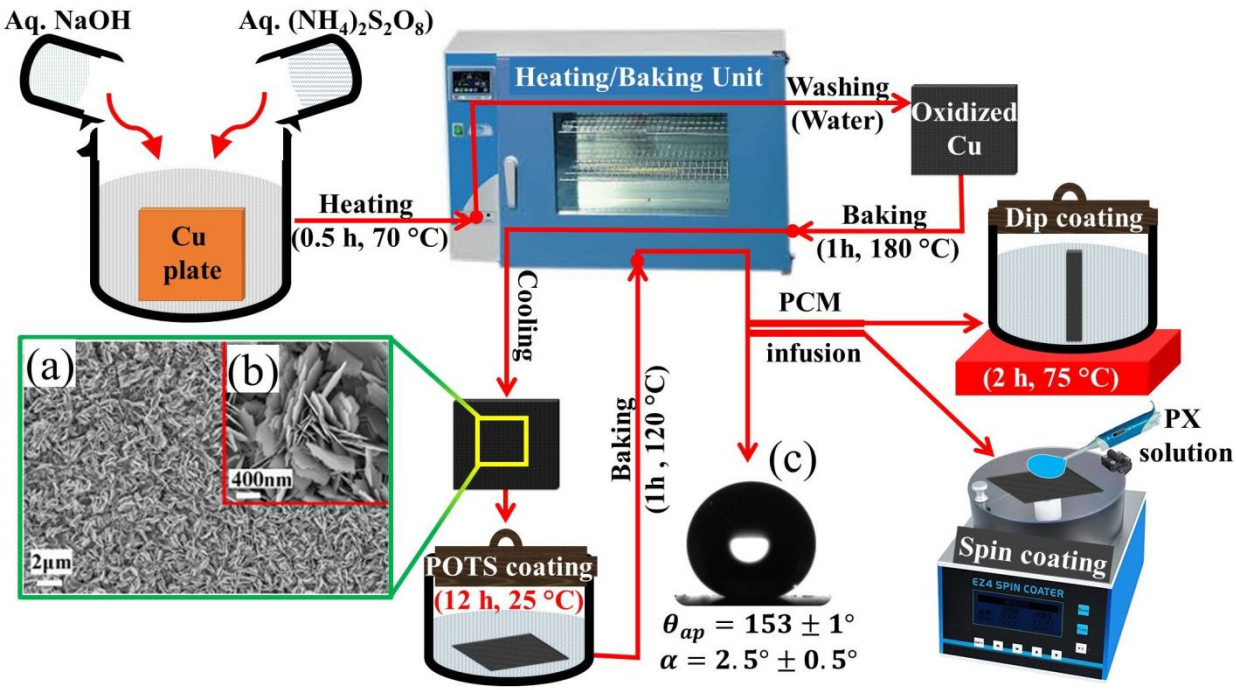

Figure 1. Schematic of the fabrication procedure of the PC-SLIPSs. The sheet-like nanostructures consisting of cupric oxide nanoporous network has been obtained on copper

plate, as shown by SEM images in (a) and (b).[9] The apparent contact angle and roll-off angle are shown in (c).

The different phases of paraffin wax have been characterized through differential scanning calorimetry as a function of the temperature (DSC, Perkin Elmer, DSC 8000) as shown in Figure S1 in the accompanying Supporting Information (SI). The solid phase occurs between 25-52 °C, the mush phase appears between 53-59 °C, and the liquid phase ensues at 60 °C and sustains itself above this temperature.

In dip coating, the hydrophobized nanoporous copper surface was vertically immersed for 2 h in the pool of paraffin wax maintained at 75 °C and then slowly removed from the pool, followed by vertically hanging the PC-SLIPSs in the oven at 75 °C for 30 minutes (thermal annealing), and then drying at ambient temperature for several minutes. Subsequently, the surface morphology was analyzed using optical microscopy in the solid phase at 25 °C and the liquid phase at 60 °C (Figure 2), as well as surface roughness (R_a and R_z; R_a: average surface roughness, R_z: difference between highest peak/bump and deepest valley/dent) was determined by non-contact optical profiler. In the solid phase at 25 °C, the surface morphology appears with the presence of non-uniform and random microfeatures comprising of bumps and dents (Figure 2a) with $R_a = 1.8 \pm 0.4$ μm and $R_z = 4.9 \pm 1$ μm (see surface profiles in Figure S2 in the SI). Consequently, strong pinning is observed with a high sliding angle of 70±5° (Figure 2b), which corresponds to the high adhesion Wenzel (HAW) state in the solid phase. Upon transition to the liquid phase at 60 °C, an even and smooth liquid layer is observed (Figure 2c). In this phase, the sliding angle is 2±1° (Figure 2d), demonstrating high droplet mobility, i.e., efficient slippery state with virtually no pinning, but on the penalty of

presence of excess paraffin that partially covers the wetting ridge,[41] as highlighted (red square) in Figure 2d (also see Video S1).

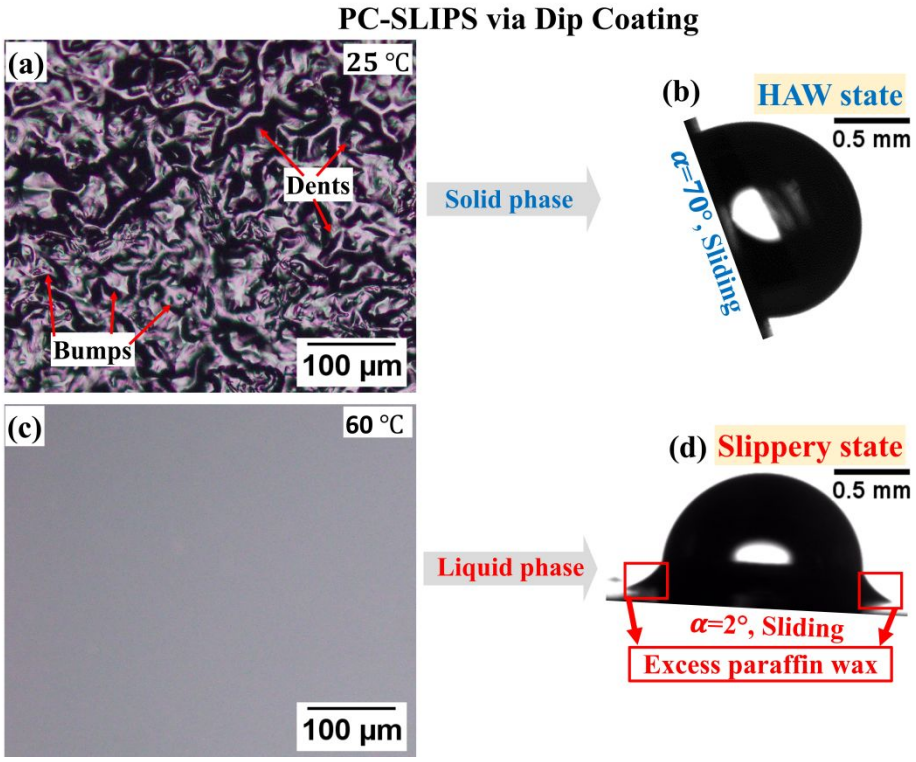

Figure 2. Dip-coated PC-SLIPSs. Optical microscopy of the surface microfeatures of the PC-SLIPSs in the solid phase at 25 °C (a) and the liquid phase at 60 °C (c). Contact angle goniometry for a 5 μl water droplet at the sliding angle α in the solid phase at 25 °C (b) and the liquid phase at 60 °C (d).

It should be noted that, the droplet is able to slide on the dip-coated PC-SLIPSs in the HAW state on behalf of minimized paraffin lodging and thermal annealing as compared with the previous reports.[33,35] However, even after trying these fabrication steps, dip-coating procedure could not guarantee the optimal quantity of paraffin wax in the liquid phase, i.e., fine control of excess lubricant. In order to optimize the overall design of the PC-SLIPSs, the amount of paraffin wax has been controlled via spin-coating. In addition, the microfeatures of

the PC-SLIPSs in the solid phase have further been controlled through thermal annealing, as illustrated in Figure 3. The details of the optimization design are elaborated in Section S2 in the SI. Spin-coating procedure was challenging to be executed at ambient temperature because of the fast solidification of the paraffin wax. In order to retain the liquid phase of paraffin wax, we introduced xylene as a solvent[42] that slows down the solidification and allows effective spin-coating. After spin-coating, as-prepared PC-SLIPSs were dried overnight that led to the completely-pinned Wenzel state (droplet immobility) because of the microstructural defects arising from the segregated paraffin wax crystals, particularly after the complete evaporation of xylene, as can be seen in Figure S4 in the SI.

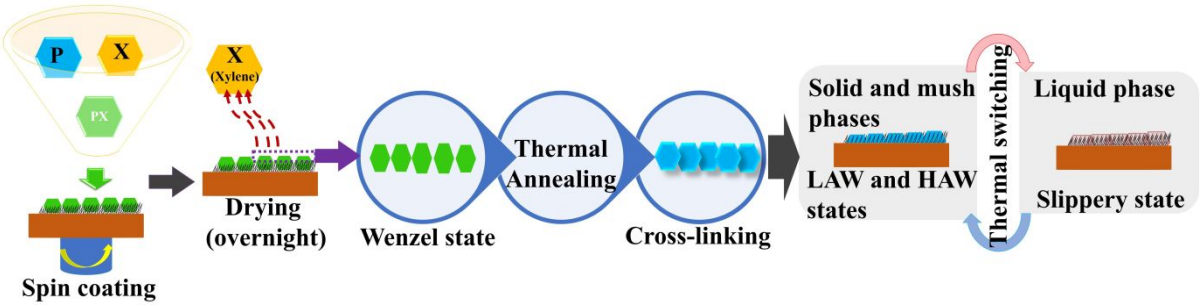

Figure 3. Schematics of the impregnation steps of the PC-SLIPSs, including spin coating, drying, thermal annealing and thermal switching. Paraffin-xylene mixture was used for the spin-coating method.

In an attempt to further refine the surface sturctures after spin coating and overnight drying, thermal annealing that consists of heating the surfaces at 75 °C for 6 h was further applied. The annealing process mitigates the presence of structural defects (micro-bumps and micro-dents) between the parted paraffin crystals on the PC-SLIPSs. Besides spin coating and thermal annealing, a threshold amount of paraffin wax in paraffin-xylene solution below which slippery state cannot be achieved even in the liquid phase has been reported (see Figure S5 in the SI). Hence, for the optimum design, the right amount of paraffin wax must be applied to the surface followed by spin coating and thermal annealing. The solid phase of

the optimized PC-SLIPSs demonstrates significantly diminished micro-structural defects (Figure 4a), leading to R_a = 0.39±0.1 µm and R_z = 0.92±0.2 µm (see surface profiles in Figure S6 in the SI). Owing to the reduced surface roughness, droplet pinning is less strong and the droplet mobility is significantly enhanced, showing a decrease in the sliding angle down to 30±10° (Figure 4b) which corresponds to the low adhesion Wenzel (LAW) state overcoming the complete pinning of the droplets at inclination angles of 90° earlier reported in the literature.[33,35] In the liquid phase (Figure 4c), the surface presents slippery state without excess of paraffin wax, showing the sliding angle of 4±1° (Figure 4d compared to the excess of lubricant reported in Figure 2d). The sliding angle is slightly higher than that of the dip-coated PC-SLIPSs in the liquid phase (2±1°), which is attributed to the less amount of paraffin wax available on the surface (see Video S2).

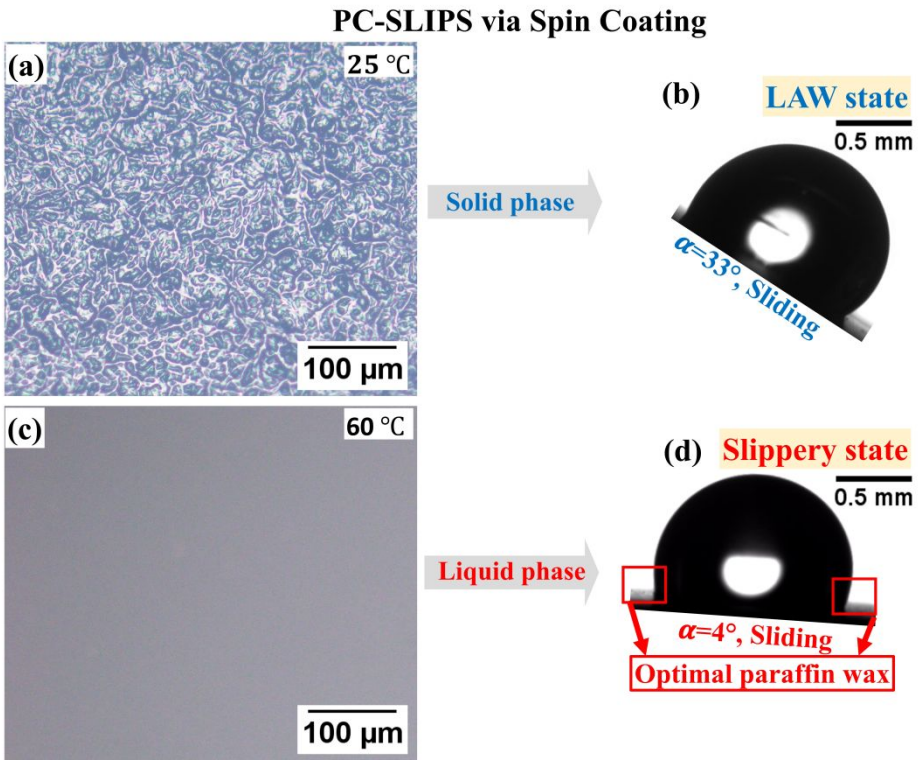

Figure 4. Spin-coated PC-SLIPSs after thermal annealing. Surface microfeatures of the PC-SLIPSs in the solid phase at 25 °C (a) and the liquid phase at 60 °C (c). Contact angle goniometry for a 5 µl water at the sliding angle α in the solid phase at 25 °C (b) and the liquid

phase at 60 °C (d). Note the absence of excess of lubricant when comparing Figure 4d to Figure 2d.

To address the surface topography and wetting properties more systematically, the topographic configuration of the PC-SLIPSs at different surface temperatures has been further examined, as shown in Figure 5. As the temperature increases from 35 to 45 °C, the surface topography undergoes a gradual change because of the solid-solid transition (see Figure S1 in the SI), whereas a prominent change in the topography begins to appear between 53-59 °C during the solid-liquid transition (mush phase). Because of the coexistence of solid-liquid mixture during the mush phase,[43] the interspacing of micro-bumps and micro-dents increases. Some micro-bumps and micro-dents are also engulfed by the liquid phase, which is highly noticeable between 56-58 °C. The topographic features eventually disappear at the melting temperature of 60 °C (Figure 4c), resulting in a smooth, uniform and thin liquid layer.

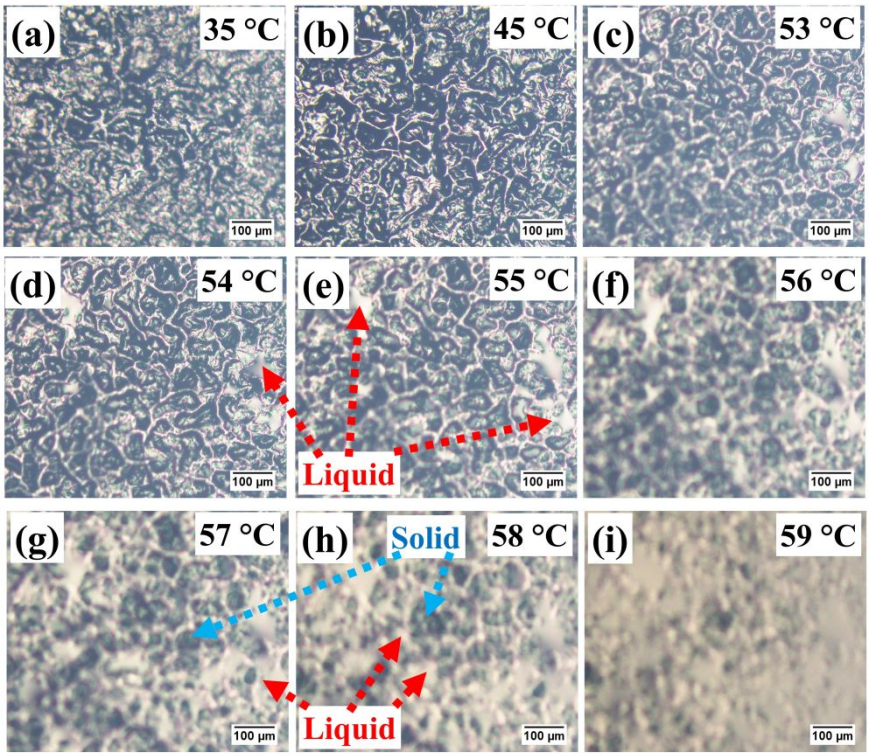

Figure 5. Optical microscopy of the PC-SLIPSs at varying temperatures from 35 to 59 °C, illustrating the surface morphologies of the solid phase (a-b) and mush phase (c-i), while the liquid phase is shown in Figure 4c. In the images corresponding to the mush phase, red arrows indicate regions of the solid to liquid phase change, while the blue arrows indicate the solid phase. Scale bars are 100 µm.

To further characterize the surface stability and the surface wettability of the PC-SLIPSs at different temperatures, the spreading coefficient S_{pw} predicting the occurrence of cloaking (i.e., the tendency of the lubricant to encapsulate the water droplet) and the varying interfacial tensions of paraffin wax-air (σ_{pa}) and water-air (σ_{wa}) have been theoretically calculated. In order to quantitatively predict the occurrence of cloaking, the spreading coefficient S_{pw} is estimated. S_{pw} is defined with respect to the individual interfacial tensions of paraffin wax-air (σ_{pa}), water-air (σ_{wa}), and water-paraffin wax (σ_{wp}) as in Equation 1.[2,34,44]

$$S_{pw} = \sigma_{wa} - \sigma_{wp} - \sigma_{pa} \quad (1)$$

Upon droplet shedding from the surface, cloaking may result in direct deterioration of the SLIPSs as the shedding of a droplet carries the lubricant away inducing the depletion of the lubricant. A robust surface where the lubricant does not cloak a water droplet should meet the criterion of negative spreading coefficient as $S_{pw} < 0$, and contrarily, $S_{pw} > 0$ shows the occurrence of cloaking.[17] The surface free energy of the paraffin wax-air (σ_{pa}) at higher temperatures was measured by Kobald et al.,[45] and was empirically extrapolated for lower temperatures by Piscitelli et al.[46], as shown in Figure 6a, which also includes the temperature-dependent surface tension for water-air σ_{wa}. σ_{wp} is calculated using Equation 2 with the help of dispersion forces of interacting substances, i.e., γ^d_{wa} is 21.8 mN/m[34] and γ^d_{pa} is 33.8 mN/m (note that for non-polymeric substances $\sigma_{pa} \approx \gamma^d_{pa}$.[34]

$$\sigma_{wp} = \sigma_{pa} + \sigma_{wa} - 2[\gamma^d_{pa}\,\gamma^d_{wa}]^{1/2} \qquad (2)$$

Therefore, σ_{wp} and S_{pw} are calculated and the results are shown in Figure 6b. The negative spreading coefficient ($S_{pw} < 0$) within the given temperature range indicates that the lubricant (paraffin wax) does not cloak a water droplet. Thus, the criterion of the cloaking-controllable SLIPSs is effectively met with paraffin wax which, on behalf of poor miscibility, lack of chemical affinity towards water and high surface tension, renders the smart surfaces more stable than low surface tension oils.[17,19]

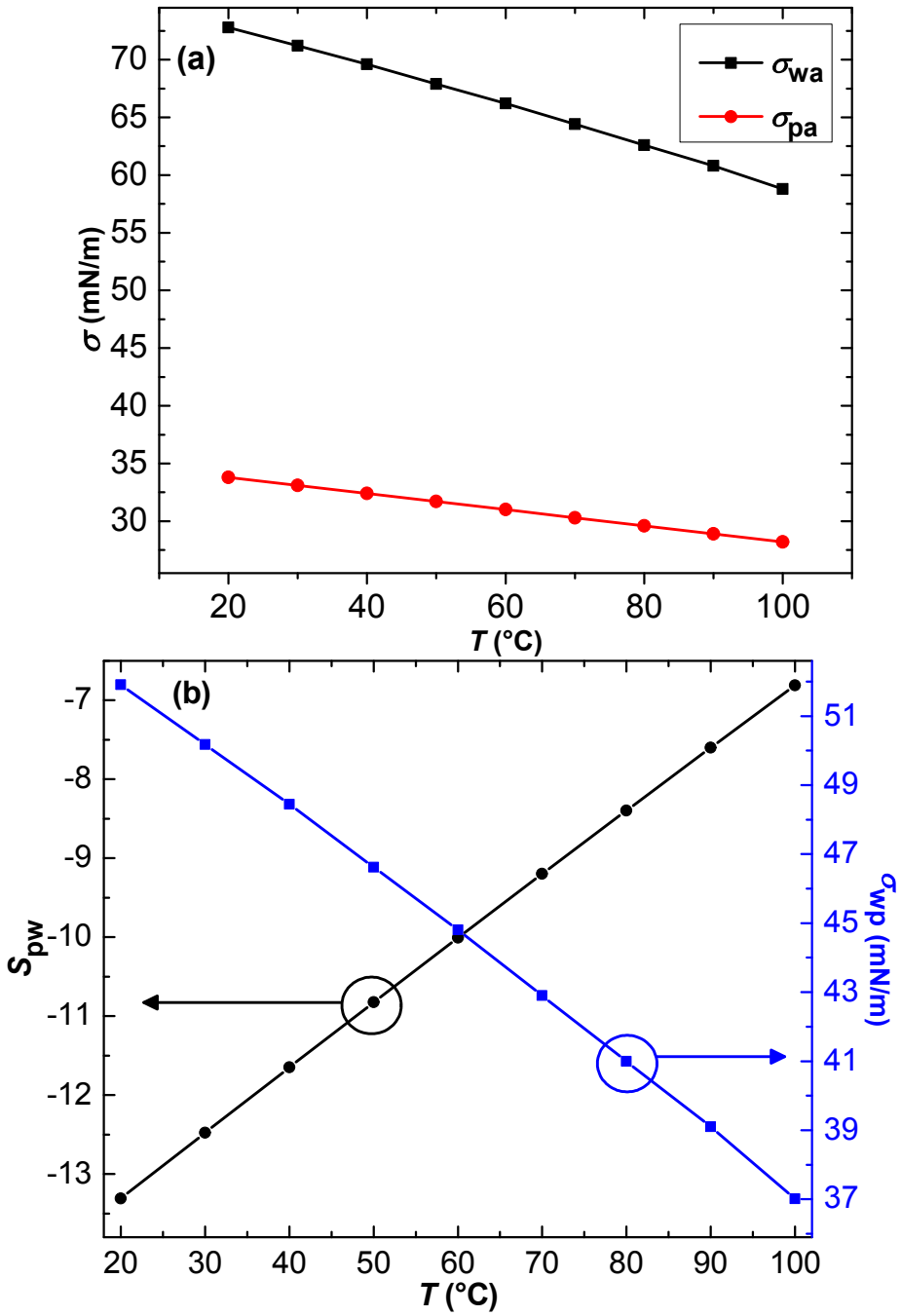

Figure 6. (a) Interfacial tensions of water-air (σ_{wa}) and paraffin wax-air (σ_{pa}) are represented. (b) Spreading coefficient, S_{pw}, calculated via Equation 1 and interfacial tension of the water-paraffin wax, σ_{wp} (mN/m), estimated via Equation 2, both as a function of temperature, T (°C). A negative spreading coefficient as $S_{pw} < 0$ at any given temperature indicates the absence of cloaking.

We note here that the relatively thinner coating was enabled by the optimal quantity of the paraffin wax achieved through the fabrication steps, i.e., spin coating and thermal annealing, which is of paramount importance to shift the completely pinned Wenzel state[32-35] or HAW state (as reported above for the dip-coated PC-SLIPSs) into the LAW state particularly in the solid phase. It is thereafter inferred that the distinct characteristics of the PC-SLIPSs, and more importantly the droplet-surface interactions, can be tuned to achieve different wetting states, i.e., strongly pinning (HAW state), weakly pinning (LAW state) and virtually non-pinning (slippery state). Hereinafter, all the results are presented on the thermally annealed spin-coated PC-SLIPSs with optimal paraffin wax.

Thermo-responsive Switchable Wettability of the PC-SLIPSs. Figure 7 shows the comprehensive characterization results of the thermally annealed spin-coated PC-SLIPSs at various temperatures including the apparent contact angle, sliding angle, and contact angle hysteresis.

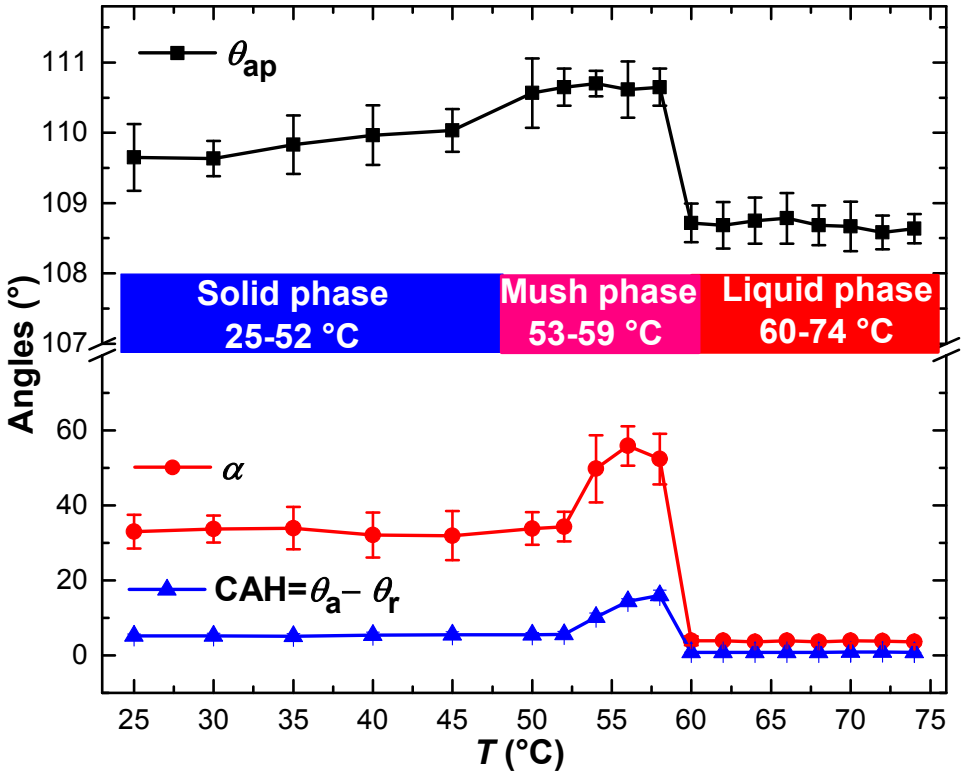

Figure 7. Thermo-responsive wetting characteristics as apparent contact angle θ_{ap} (filled black squares), sliding angle α (filled red circles), and contact angle hysteresis CAH (filled blue triangles) on the PC-SLIPSs. The solid phase depicts the LAW state, the mush phase comparatively undergoes a HAW state, while the liquid phase induces the slippery state. Error bars represent the standard deviation of five independent experiments.

Of utmost importance is the switchable wetting behavior of the PC-SLIPSs depending on the solid, mush and liquid phases controlled through temperature. The value of apparent contact angle does not vary to a great extent, i.e., fluctuates within ±2° across the entire range of temperatures studied. However, switchable wettability reported here is of practical consideration when investigating the droplet mobility. Paying special attention to the sliding angle α, a decrease from 30±10° down to 4±1° occurs when comparing the solid phase (between 25 and 52 °C) to the liquid phase (at 60 °C and above), as represented by the red curve in Figure 7. We note here that in between the solid and liquid phases the mush phase

ensues (between 53 and 59 °C), which further hinders the droplet mobility with higher sliding angles of 55±5°, a characteristic of the HAW state. This switchable wetting behavior is strongly correlated to the surface topography depending on the temperature. In the solid phase, topographic changes occur slightly (Figure 5a and 5b) so that the apparent contact angle and sliding angle are barely influenced. Conversely, the mush phase undergoes abrupt topographic changes with the presence of solid-liquid phases, which tend to enhance the droplet pinning as a consequence of the irregular and non-uniform topography (Figure 5c-i). For higher substrate temperatures, the liquid phase ensues the provision of the lowest achievable sliding angle of practical interest for high temperature applications. By gradually varying the temperature, the wettability of the PC-SLIPSs can be efficiently tuned in the LAW, HAW and slippery states at solid, mush and liquid phases, respectively.

Depicted in Figure 7 (blue curve) is the contact angle hysteresis (CAH), which is quantitatively defined as the difference between advancing contact angle θ_a and receding contact angle θ_r at the instant when a droplet starts moving. The CAHs on the PC-SLIPSs are also dependent on the nature of phases, i.e., solid, mush or liquid. Particularly, the CAH is 7±2° in the solid phase (LAW state), and then slightly increases in the mush phase with a CAH of 13±2° (HAW state) and then becomes as low as 1±0.5° in the liquid phase (slippery state).

Contact Line Dynamics and Depinning Force of the PC-SLIPSs. To provide further insights regarding the droplet adhesion/pinning in the solid, mush and liquid phases, we address the droplet evaporative behavior, paying special attention to the contact line dynamics and its depinning force. By looking at the temporal evolution of the droplet profile evaporating and more particularly at the contact line, the greater (pinning) or lesser (slipperiness) affinity of the liquid to the substrate can be inferred.[47] Such affinity is dictated

by the wettability[48] and the structure[49] of the surface. On one hand, high energy surfaces (hydrophilic), having either smooth or heterogeneous topography, typically induces stickiness characterized by the predominant pinning of the contact line prompting evaporation in the constant contact radius (CCR) mode.[50] On the other hand, on smooth low-energy surfaces (hydrophobic), the characteristic receding motion of the contact line (depinning) with the droplet evaporating in the constant contact angle (CCA) mode ensues.[51] In addition to these reported modes, a mixed mode typically ensues at the end of the evaporation[52] and a stick-slip mode occurs in the presence of low energy surfaces with small defects or structures.[53] In this work, the dynamics of the contact line of sessile water droplets of 4 µl in volume are examined on the PC-SLIPSs at different temperatures, i.e., different phases of the PCM. Then, the evolution of the contact radius R (mm) is quantitatively extracted and plotted as a function of time t (min). Figure 8 shows the evaporation-driven transient profiles along with the extracted temporal evolution of R on the pristine copper (Figure 8a) and on the PC-SLIPSs at different temperatures including the solid phase (Figure 8b), the mush phase (Figure 8c) and the liquid phase (Figure 8d). We note here that experimental observations of droplet evaporation cannot be used to accurately estimate the CAH as upon droplet deposition, and droplet adopts an apparent contact angle which is lower than that of the advancing one while evaporation cannot either accurately predict the receding contact angle as per the different dynamics involved. The receding contact angle was though utilized to estimate the contact line depinning force as proposed by Sarshar et al.,[7] and Xu et al.[8]

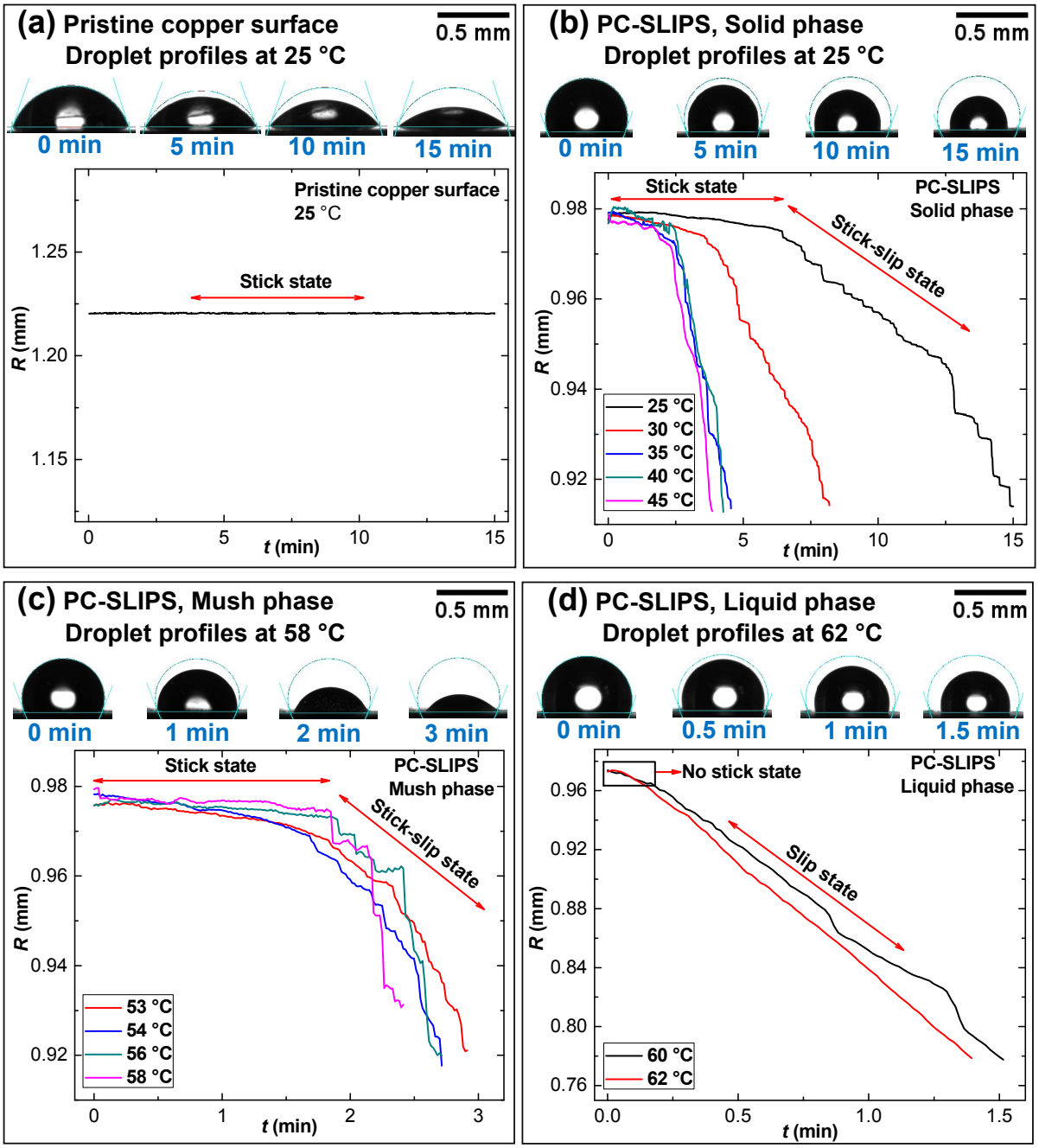

Figure 8. Droplet profile and temporal evolution of the contact radius *R* (mm) plotted as a function of time *t* (min) on the pristine copper at 25 °C (a) and the PC-SLIPSs at different temperatures including the solid phase (LAW state) (b), the mush phase (HAW state) (c), and the liquid phase (slippery state) (d). Scale bars are 0.5 mm.

On a pristine copper surface, a droplet evaporates in the CCR mode where the contact line remains pinned and the contact angle decreases to account for the decrease in the droplet volume throughout the entire lifetime of the droplet, as shown in Figure 8a. Evaporation in the CCR mode is typically prompted on high-surface-energy rough/structured substrates.[6] When looking into the temporal evolution of droplets evaporating on the PC-SLIPSs, different evaporative behaviors are observed when compared to the pristine copper surface, and more importantly when comparing the different phases of the paraffin wax itself. On the PC-SLIPSs in the solid phase, the contact line remains pinned to the surface during approximately 30 to 40% of the droplet lifetime where droplets initially evaporate in the CCR mode. Thereafter, the contact line recedes, i.e., depin, and evaporation takes place in the stick-slip mode as the multiple receding jumps of the contact line shown in Figure 8b.[48-49] The initial CCR stage signifies the pinning/stickiness of the solid phase to some extent. Here, the paraffin wax allows the transition from the CCR to CCA mode (with stick-slip motions) since it significantly lowers the surface energy when compared to bare copper. The qualitative behavior is consistent for the different ranges of temperatures between 25 and 45 °C, and the shorter depinning trend appears at higher temperatures due to enhanced evaporation. In the mush phase (53-59 °C), the CCR mode ensues during a prolonged period, i.e., approximately 60% of the droplet lifetime (Figure 8c), when compared to the solid phase (Figure 8b). After depinning, the contact line recedes in a stick-slip fashion with greater magnitude of the jumps/slips of the contact line than those taking place in the solid phase. The more dominant initial pinning stage and the greater magnitude of the jumps/slips of the contact line in the following receding stage evidence the greater adhesion in the mush phase when compared to the solid phase. This is due to the change in the structure of the paraffin wax during the melting, i.e., the coexistence of solid-liquid phases creating irregular and heterogeneous topography where the pinning of the contact line is prompted. For temperature

above that of the mush phase, the paraffin wax rests as the smooth and homogeneous liquid phase. Upon the deposition of a droplet on the PC-SLIPSs in the liquid phase, there is virtually no pinning and the continuous receding of the contact line in the CCA ensues during the entire droplet lifetime, in agreement with the works of Guan *et al.,* and Wells *et al.*[53-54]

The magnitude of the pinning can further be characterized quantitatively by estimating the depinning force, F_d (mN/m),[7,8] which is defined as the force per unit length at which the contact line begins to move, as follows:

$$F_d = \sigma_{aw} (\cos\theta_{re} - \cos\theta_{ap}) \quad (3)$$

where σ_{aw} is the air-water surface tension. Figure 9 shows the depinning force F_d with respect to the surface temperature and the phase of the PC-SLIPSs.

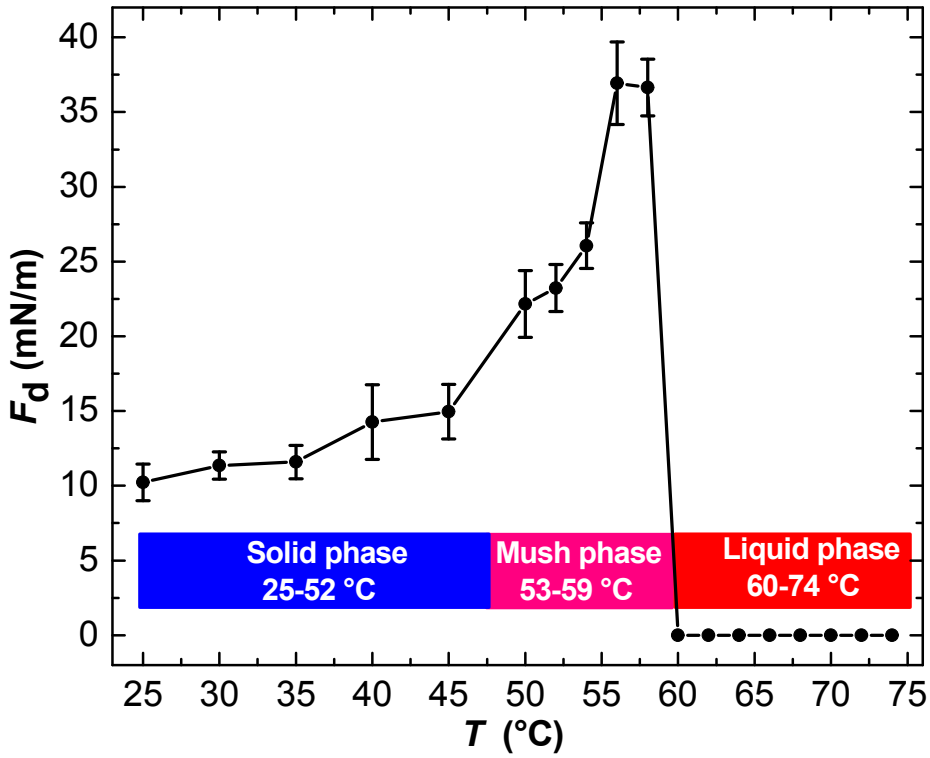

Figure 9. Contact line depinning force, F_d (mN/m), of an evaporating droplet on the PC-SLIPSs at various surface temperatures T (°C) and phases of the PC-SLIPSs. Error bars represent the standard deviation of five independent experiments.

The depinning force also clearly signifies the important differences in pinning depending on the surface temperature and phase of the PC-SLIPSs. Particularly, the PC-SLIPSs in the solid phase yields depinning forces in the range of 10 to 15 mN/m, i.e., LAW state. In the mush phase, the depinning force increases up to 37 mN/m, indicating significantly enhanced pinning, i.e., HAW state. In the liquid phase, the depinning force is negligible (close to 0 mN/m), indicating the highly slippery state. The results show that the depinning force is temperature-dependent, stressing the significance of the thermo-responsive switchable wettability of the PC-SLIPSs.

Thermo-responsive Droplet Size Distribution during Condensation on the PC-SLIPSs.

According to the wetting regimes prompted by the present thermo-responsive PC-SLIPSs, a wide range of simultaneous applications can be opened up depending on the operation temperature and conditions, encompassing water adhesion and sliding. As paraffin wax is environmentally friendly, such PC-SLIPSs are deemed to be highly beneficial for many applications, such as water collection. Considering such applications, the PC-SLIPSs have been examined as condensing surfaces at standard atmospheric conditions (1 atm in pressure). The experiments have been done in a custom-built water vapor condensation unit as shown in Figure S7 in the SI. The durability and stability of the thermos-responsive wetting properties of the PC-SLIPSs have been estimated through rigorous condensation tests consisting of 40 experimental runs (i.e., 20 for liquid phase and 20 for solid phase) that lasted for around 280 min in total. After condensation tests, the apparent contact angle of a water droplet on the PC-SLIPSs has been found to be 107±0.5° in both phases, which is almost equal to that determined before condensation tests (108±0.5°). It can be inferred that if there were a mass loss of paraffin from the surfaces, the apparent contact angle should have been equal to that on the hydrophobized nanoporous copper substrate which is 153±1° (Figure 1c).

For further comparison, the condensation patterns on the pristine copper surface and PC-SLIPSs are shown in Figure 10. On the pristine copper surface, the condensate nucleates, grows and coalesces, forming irregular droplets covering the surface in a conventional filmwise condensation fashion (Figure 10a-10c). In contrast, on the PC-SLIPSs, the continuous shedding of spherical droplets is prompted both in the solid (Figure 10d-10f; see also Video S3 in the SI) and liquid phases (Figure 10g-10i; see also Video S4 in the SI). The condensation mechanism of either phase on the PC-SLIPSs follows nucleation (Figure 10d for the solid phase and Figure 10g for the liquid phase), growth (Figure 10e for the solid phase and Figure 10h for the liquid phase), and shedding of droplets (Figure 10f for the solid phase and Figure 10i for the liquid phase), which is the characteristic of continuous dropwise condensation.[55] More specifically, when the PC-SLIPSs are in the solid phase, water droplets grow by direct condensation and coalescence to sizes in the order of a millimeter followed by droplet shedding (Video S3 in the SI), which is in agreement with what has been reported on smooth low adhesion hydrophobic surfaces.[56,57] As opposed to the solid phase, smaller droplets with sizes in the submillimeter range (Video S4 in the SI) shed from the surface of the PC-SLIPSs in the liquid phase, which is also a clear indication of the slippery state.[58]

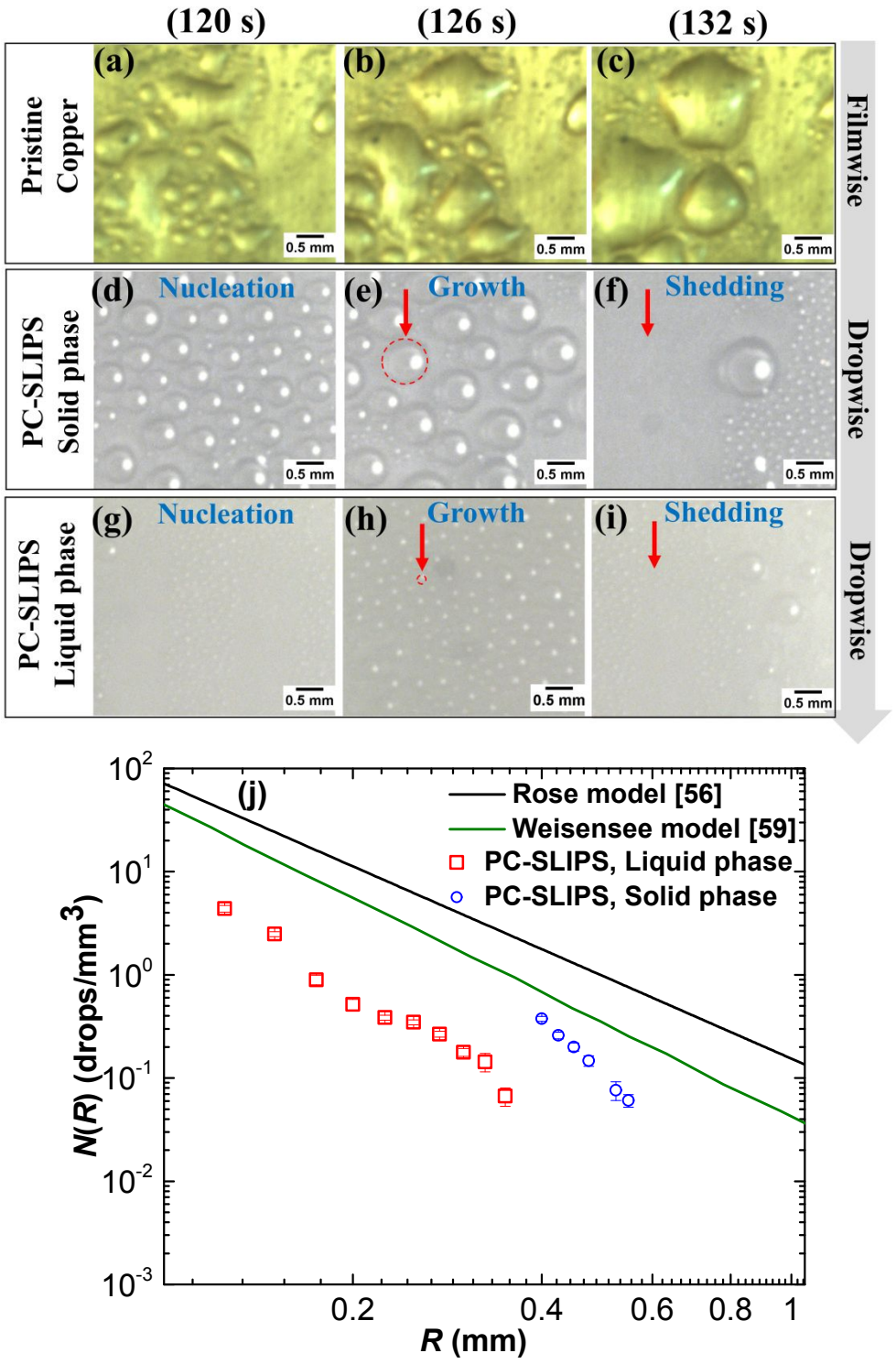

Figure 10. Condensation patterns on the pristine copper surface (a-c), the PC-SLIPSs in the solid phase (LAW state) (d-f), and the PC-SLIPSs in the liquid phase (slippery state) (g-i). The slightly greenish color of the pristine copper surface is because of the light provided in the experimental setup. Red-dashed circles show the droplets and their shedding down the

surfaces. Scale bars are 0.5 mm. Droplet number density $N(R)$ (drops/mm^3) versus droplet radius R (mm) in the solid phase (red circles) and the liquid phase (blue squares) of the PC-SLIPSs (j). The theoretical correlations for dropwise condensation proposed by Rose *et al.*[56] and power-law fitting introduced by Weisensee *et al.*[59] are included for comparison.

The results (Figure 10d-i and Videos S3-S4 in the SI) show that the thermo-responsive droplet size distributions have been achieved for the first time on the PC-SLIPSs. As a further quantitative analysis of the dynamic condensation and to demonstrate the distribution of the different droplet sizes depending on the phase of the PC-SLIPSs, we make use of the droplet number density $N(R)$ (drops/mm^3) as widely accepted in the literature.[56,59] The droplet number density $N(R)$ can be estimated from the total number of droplets N_d of a given size R divided by the surface area A (10 × 10 mm^2) and the size of the droplets R as follows:

$$N(R) = (N_d/A)/R \tag{4}$$

To represent the effect of the droplet size distribution on the shedding behavior, the $N(R)$ values are averaged from three different experimentations right before a shedding event ensues in both the solid and liquid phases, i.e., when the droplets experience their greater sizes. Figure 10j plots the droplet number density $N(R)$ with respect to the droplet radius R, which is also compared with the models suggested by others.[56,59] The results show that the maximum radius for droplet shedding shifts from as large as 0.53 mm in the solid phase down to as small as 0.35 mm in the liquid phase. In addition, a higher droplet number density in the liquid phase than that in the solid phase of the PC-SLIPSs is remarkably shown. We note a good qualitative agreement between the droplet number density of the PC-SLIPSs and the theoretical correlations suggested by the Rose[56] and Weisensee models.[59] The deviation of the experimental data from the theoretical prediction is attributed to the fact that the experimental data were chosen at the moment right before the onset of shedding, i.e., when

the droplets display their greater sizes, and the precise estimation of droplet sizes in the order of tens of micrometers was also difficult. Dropwise condensation on regular LISs or SLIPSs have demonstrated the different maximum size of the shedding droplets depending on the condensing liquid even for low surface tension fluids.[60,61] Meanwhile, the type of lubricant was found not to affect the droplet size distribution for water condensing on the SLIPSs but to affect the droplet shedding velocity.[59] This was also the case for low surface tension fluids where, for the same hydrophobic nanostructured surface, the lubricant impregnated did not influence the maximum size of the shedding droplets.[61] Further, whereas Maeda et al. observed a quantitative change in the droplet size distribution when comparing the type of hydrophobic structured surface underneath, the clear shift on the droplet size distribution range and that of the maximum droplet size from approximately 600 μm to 300 μm was not reported.[62] The results show that the unique thermo-responsive switchable wettability allows the dropwise condensation in both the solid and liquid phases of the PC-SLIPSs, with the additional features of the control of droplet sizes and droplet number density that can also lead to effective performance for condensation heat transfer applications.[56,59] We note here that the wide range of PCMs and melting temperatures call for further exploration for the specific condensation heat transfer applications.

CONCLUSIONS

PC-SLIPSs (phase-change slippery-liquid infused porous surfaces) have been presented paying special attention to the microscopic features, the thermo-responsive wettability and the contact line depinning dynamics, as well as the condensation patterns. The PC-SLIPSs were fabricated via spin coating and subsequent thermal annealing of an optimized amount of paraffin wax providing decreased surface adhesion (low adhesion Wenzel state) and absence

of excess of paraffin wax when compared to earlier reported dip coating procedure inducing high adhesion Wenzel state. As a result, the contact line dynamics appears to be weakly pinned in the solid phase (low adhesion Wenzel state), strongly pinned in the mush phase (high adhesion Wenzel state), and virtually non-pinned in the liquid phase (slippery state). Last, the thermo-responsive nature of the condensation patterns, i.e., the different size of the shedding droplets between the solid and liquid phases, has been demonstrated and supported on the premise of low adhesion Wenzel and slippery states. Especially, a larger droplet density in the liquid phase switches towards smaller droplet density in the solid phase. Based on the imposed temperatures, tunable wettability is therefore the distinct feature of the PC-SLIPSs driven by the solid, mush and liquid phases.

EXEPERIMENTAL SECTION

Materials. Copper plate (15 mm×15 mm×0.4 mm) has been employed as a substrate (pristine copper surface). Paraffin wax (melting temperature of 60-62 °C) and ammonium peroxide [$(NH_4)_2S_2O_8$)] were bought from Sinopharm Chemical Reagent. Absolute ethanol (CH_3CH_2OH), acetone (C_3H_6O), xylene (C_3H_8) and sodium hydroxide (NaOH) were bought from Shanghai Lingfeng Chemical Reagent. 1H, 1H, 2H, 2H-perfluorooctyltriethoxysilane (POTS) having purity of 97% was purchased from Alfa Aesar.

Fabrication of Hydrophobic Porous Surface and the Paraffin Wax Coating. The porous copper surface was prepared via chemical oxidation by following our previous work,[9] which is explained schematically in Figure 1. Prior to oxidation, copper plate was cleaned by acetone, and then dipped (reaction time: 1 hour at 70 °C) into highly alkaline solution of aqueous sodium hydroxide (2.5 M) and aqueous ammonium persulfate (0.1 M), serving as pH controller and oxidizing agent, respectively. Subsequently, surfaces were rinsed with distilled

water, dried by nitrogen gas and then baked at 180 °C to ensure the formation of cupric oxide, providing deep black and velvety appearance of the nanostructures yielding average surface roughness of 1.79 μm.[9] The nanoporous copper surfaces were hydrophobized by immersing in 1% ethanol solution of POTS (1H,1H,2H,2H-perfluorooctyltriethoxysilane) for 12 h at ambient temperature, and subsequently baked at 120 °C. Afterwards, the paraffin wax was dissolved using xylene as a solvent, resulting in paraffin-xylene (hereinafter refer to as PX) solution. Regardless of critical stoichiometric quantities, the concentration of solution has been arbitrarily set such that the liquid phase of paraffin wax could be sustained at ambient temperature, thus enabling to properly make use of the spin coating technique. Accordingly, 9.6 wt% (1.4 g), 10.2 wt% (1.5 g) and 10.8 wt% (1.6 g) paraffin wax were dissolved in 15 ml (12.67 g) xylene. For spin coating, 100 μL PX solution was filled in digital pipette, and was poured down onto the porous substrates followed by the spinning at 4000 rpm for 30 s, and this procedure was repeated three times ensuring that the entire sample was fully coated. Spin coating helped eliminate the excess of paraffin wax. After spin coating, the surfaces were dried overnight at ambient temperature so as to evaporate the xylene, and afterwards, they were subjected to thermal annealing at 75 °C for 6 h, which not only ensures full impregnation of nanopores but also develops continuous cross-linking between the segregated paraffin wax crystals.

Characterization and Experimental Setup. Surface morphology of the PC-SLIPSs was characterized using optical microscopy (OLYMPUS BX51M) which was coupled with a Peltier device to control the temperature of the PC-SLIPSs. Surface roughness of the PC-SLIPSs has been determined with the help of non-contact optical profiler (ZETA 20) at ambient temperature. The apparent contact angles and sliding angles were determined through optical contact angle (OCA) goniometer (OCA-20) by using water droplet size of 5 μL. The size of the droplets was always kept below the capillary length to avoid the effect of

gravity on the droplet shape. In order to measure the contact angles at higher temperatures, the temperature control stage of OCA was set at the desired temperatures by circulating the hot water from thermostatic bath (DC-2020, CNSHP) connected to a water pump (PLD-1205) running at a flow rate of 29 ml/s.

To address the contact line dynamics, droplet evaporation was carried out at the same temperature control stage of the OCA, and the droplet-profiles were recorded by the OCA camera. The droplet size was kept to be 4 μL for all evaporation tests. Thereafter, the droplet base diameter, receding angle in evaporation θ_{re} and apparent contact angle θ_{ap} were extracted from the OCA post-processing procedure. To estimate the depinning force, θ_{ap} has been taken as the initial apparent contact angle, while θ_{re} has been taken at the moment when the first slip motion occurs on the PC-SLIPSs.

Water vapor condensation test were carried out through a custom-built condensation unit, as shown in Figure S7 in the SI. The steam enters the vapor chamber from the steam generator. The steam temperature was 99 ± 1 °C which was measured via a T-type thermocouple (as shown in Figure S7 in the SI) suspended in the vapor chamber. A copper block (20 mm×20 mm×5 mm) was employed whose square-shaped front head opens into the vapor chamber, while the rear end was welded with a chiller (cold water heat exchanger) having dimensions of 40 mm×40 mm×10 mm. The chiller was connected with thermostatic bath (DC-2020, CNSHP) to provide cold water. Onto the front head of copper block, the PC-SLIPSs were attached through conductive thermal grease. The temperatures on the PC-SLIPSs were estimated through a thermocouple (T-type) inserted into the copper black at a distance of 0.4 mm from its front head. By fixing the temperature of the chiller water at 20 °C and 55 °C, the condensation patterns in solid phase (surface temperature of 25 °C approximately) and liquid phase (surface temperature of 62 °C approximately), respectively, were recorded through HD camera.

ASSOCIATED CONTENT

Supporting Information

Differential scanning calorimetry of paraffin wax (Section S1). Design optimization of the PC-SLIPSs (Section S2). Water vapor condensation unit (Section S3). Excess paraffin wax on the PC-SLIPSs (Video S1). Optimal paraffin wax on the PC-SLIPSs (Video S2). Dropwise condensation patterns on the PC-SLIPSs in the solid phase (Video S3). Dropwise condensation patterns on the PC-SLIPSs in the liquid phase (Video S4).

AUTHOR INFORMATION

Corresponding Author

Email: zhangp@sjtu.edu.cn

Notes

The authors declare no competing financial interest.

ACKNOWLEDGMENTS

This research is supported by the National Natural Science Foundation of China under the Contract No.51976117 and the National Key Research and Development Program of China under the Contract No. 2018YFA0702300. C.H.C. is supported by US National Science Foundation ENG (Directorate for Engineering) CMMI (Division of Civil, Mechanical, and Manufacturing Innovation) under Award No.1537474. We thank Mr. Jazib Ali (School of Physics, Shanghai Jiao Tong University, Shanghai, China) for his valuable help in spin-coating during sample preparation. A few characterizations are conducted in the AEMD of Shanghai Jiao Tong University.

REFERENCES

(1) Archer, R.J.; Becher-Nienhaus, B.; Dunderdale, G.J.; Hozumi, A. Recent Progress and Future Directions of Multifunctional (Super) Wetting Smooth/Structured Surfaces and Coatings. *Adv. Funct. Mater.* **2020**, 1907772.

(2) Hai Zhu, H.; Duan, R.; Wang, X.; Yang, J.; Wang, J.; Huang, Y.; Xia, F. Prewetting Dichloromethane Induced Aqueous Solution Adhered on Cassie Superhydrophobic Substrates to Fabricate Efficient Fog-Harvesting Materials Inspired by Namib Desert Beetles and Mussels. *Nanoscale*, **2018**, *10*, 13045-13054.

(3) Lafuma, A.; Quéré, D. Superhydrophobic States. *Nature Mater.* **2003**, *2*, 457–460.

(4) Dai, X.; Stogin, B.B.; Yang, S.; Wong, T.S. Slippery Wenzel State. *ACS Nano* **2015**, *9(9)*, 9260-9267.

(5) Bhushan B.; Nosonovsky M. The Rose Petal Effect and the Modes of Superhydrophobicity. *Phil. Trans. Royal Society A: Math. Phy. Eng. Sci.* **2010**, *368(1929)*, 4713 - 4728.

(6) Bormashenkoa, E.; Musina, A.; Zinigrad, M. Evaporation of Droplets on Strongly and Weakly Pinning Surfaces and Dynamics of the Triple Line. *Colloids Surfaces A: Physicochem. Eng. Aspects* **2011**, *385*, 235–240.

(7) Sarshar, M.A.; Jiang, Y.; Xu, W.; Choi, C.-H. Depinning Force of a Receding Droplet on Pillared Superhydrophobic Surfaces: Analytical Models. *J. Colloid Interface Sci.* **2019**, *534*, 122–129.

(8) Xu, W.; Choi, C.-H. From Sticky to Slippery Droplets: Dynamics of Contact Line Depinning on Superhydrophobic Surfaces. *Phys. Rev. Lett.* **2012**, *109*, 024504.

(9) Zhang, P.; Lv, F.Y.; Askounis, A.; Orejon, D.; Shen, B. Role of Impregnated Lubricant in Enhancing Thermosyphon Performance. *Int. J. Heat Mass Transfer* **2017**, *109*, 1229–1238.

(10) Lee, J.; Shin, S,; Jiang, Y.; Jeong, C.; Stone, H.A.; Choi, C.-H. Oil-Impregnated Nanoporous Oxide Layer for Corrosion Protection with Self-Healing. *Adv. Funct. Mater.* **2017**, *27*, 1606040.

(11) Chen, A.; Peng, X.; Koczkur, K.; Miller, B. Super-Hydrophobic Tin Oxide Nanoflowers. *Chem. Commun.* **2004**, 1964–1965.

(12) Hosono, E.; Fujihara, S.; Honma, I.; Zhou, H. Superhydrophobic Perpendicular Nanopin Film by the Bottom-Up Process. *J. Amer. Chem. Soc.* **2005**, *127(39)*, 13458-13459.

(13) Cao, L.; Hu, H.; Gao, D. Design and Fabrication of Micro-Textures for Inducing a Superhydrophobic Behavior on Hydrophilic Materials. *Langmuir* **2007**, *23(8)*, 4310–4314.

(14) Kamei, J.; Yabu, H. On-Demand Liquid Transportation Using Bioinspired Omniphobic Lubricated Surfaces Based on Self-Organized Honeycomb and Pincushion Films. *Adv. Funct. Mater.* **2015**, *25*, 4195–4201.

(15) Jeong, C.; Choi, C.-H. Single-Step Direct Fabrication of Pillar-on-Pore Hybrid Nanostructures in Anodizing Aluminum for Superior Superhydrophobic Efficiency. *ACS Appl. Mater. Interfaces* **2012**, *4*, 842-848.

(16) Villegas, M.; Zhang, Y.; Jarad, N.A.; Soleymani, L.; Didar, T.F. Liquid-Infused Surfaces: A Review of Theory, Design and Applications. *ACS Nano* **2019**, *13*, 8517-8536.

(17) Preston, J. D.; Song, Y.; Lu, Z.; Antao, S.D.; Wang, E.N. Design of Lubricant Infused Surfaces. *ACS Appl. Mater. Interfaces* **2017**, *9*, 42383-42392.

(18) Aizenberg, J. Slippery Liquid-Infused Porous Surfaces (SLIPS). *J. Ocean. Tech.* **2014**, *9,* 4.

(19) Sett, S.; Yan, X.; Barac, G.; Bolton, L.W.; Miljkovic, N. Lubricant-Infused Surfaces for Low-Surface-Tension Fluids: Promise versus Reality. *ACS Appl. Mater. Interfaces* **2017**, *9*, 36400-36408.

(20) Rao, Q.; Zhang, J.; Zhan, X.; Chen, F.; Zhang, Q. UV-Driven Self-Replenishing Slippery Surfaces with Programmable Droplet-Guiding Pathways. *J. Mater. Chem. A.* **2020**, *8*, 2481-2489.

(21) Xiao, R.; Miljkovic, N.; Enright, R.; Wang, E.N. Immersion Condensation on Oil-Infused Heterogeneous Surfaces for Enhanced Heat Transfer. *Sci. Reports.* **2013**, *3*, 1988.

(22) Dai, X.; Sun, N.; Nielsen, S.O.; Stogin, B.B.; Wang, J.: Yang, S.; Wong, T.S. Hydrophilic Directional Slippery Rough Surfaces for Water Harvesting. *Sci. Adv.* **2018**, *4(3)*, eaa0919.

(23) Kim, P.; Wong, T.S.; Jack Alvarenga, J.; Kreder, M.J.; Martinez, W.E.A.; Aizenberg, J. Liquid-Infused Nanostructured Surfaces with Extreme Anti-Ice and Anti-Frost Performance. *ACS Nano* **2012**, *6(8)*, 6569-6577.

(24) Yu, Y.; Jin, B.; Jamil, M.I.; Cheng, D.; Zhang, Q.; Zhan, X.; Chen, F. Highly Stable Amphiphilic Organogel with Exceptional Anti-icing Performance. *ACS Appl. Mater. Interfaces* **2019**, *11*, 12838-12845.

(25) Jin, B.; Liu, M.; Zhang, Q.; Zhan, X.; Fengqiu Chen, F. Silicone Oil Swelling Slippery Surfaces Based on Mussel-Inspired Magnetic Nanoparticles with Multiple Self-Healing Mechanisms. *Langmuir* **2017**, *33*, 10340-10350.

(26) Kreder, M.J.; Daniel, D.; Tetreault, A.; Cao, Z.; Lemaire, B.; Timonen, J.V.I.; Aizenberg, J. Film Dynamics and Lubricant Depletion by Droplets Moving on Lubricated Surfaces. *Phys. Rev. X.* **2018**, 8, 031053.

(27) Chen, C.; Zhou, L.; Shi, L.A.; Zhu, S.; Huang, Z.; Xue, C.; Li, J.; Hu, Y.; Wu, D.; Chu, J. Ultralow-Voltage-Driven Smart Control of Diverse Drop's Anisotropic Sliding by in Situ Switching Joule Heat on Paraffin-Infused Microgrooved Slippery Surface. *ACS Appl. Mater. Interfaces* **2020**, *12*, 1895-1904.

(28) Weng, D.; Xu, F.; Li, X.; Li, Y.; Sun, J. Bioinspired Photothermal Conversion Coatings with Self-Healing Superhydrophobicity for Efficient Solar Steam Generation. *J. Mater. Chem. A.* **2018**, *6*, 24441-24451.

(29) Wang, F.; Ding, W.; He, J.; Zhang, Z. Phase Transition Enabled Durable Anti-Icing Surfaces and its DIY Design. *Chem. Eng. J.* **2019**, *360*, 243-249.

(30) Wang, Z.; Xu, Q.; Wang, L.; Heng, L.; Jiang, L. Temperature-Induced Switchable Interfacial Interactions on Slippery Surfaces for Controllable Liquid Manipulation. *J. Mater. Chem. A.* **2019**, *7*, 18510-18518.

(31) Banuprasad, T.N.; Vinay, T.V.; Subash, C.K.; Varghese, S.; George, S.D.; Varanakkottu, S.N. Fast Transport of Water Droplets over a Thermo-Switchable Surface Using Rewritable Wettability Gradient. *ACS Appl. Mater. Interfaces* **2017**, *9(33)*, 28046-28054.

(32) Rao, Q.; Li, A.; Zhang, J.; Jiang, J.; Zhang, Q.; Zhan, X.; Chen, F. Multi-Functional Fluorinated Ionic Liquid Infused Slippery Surfaces with Dual-Responsive Wettability Switching and Self-Repairing. *J. Mater. Chem. A.* **2019**, *7*, 2172-2183.

(33) Yao, X.; Ju, J; Yang, S.; Wang, J.; Jiang, L. Temperature-Driven Switching of Water Adhesion on Organogel Surface. *Adv. Mater.* **2014**, *26*, 1895–1900.

(34) Manabe, K.; Matsubayashi, T.; Tenjimbayashi, M.; Moriya, T.; Tsuge, Y.; Kyung, K.; Shiratori, S. Controllable Broadband Optical Transparency and Wettability Switching of Temperature-Activated Solid/Liquid-Infused Nano Fibrous Membranes. *ACS Nano* **2016**, *10(10)*, 9387-9396.

(35) Wang, L.; Heng, L.; Jiang, L. Temperature-Responsive Anisotropic Slippery Surface for Smart Control of the Droplet Motion. *ACS Appl. Mater. Interfaces* **2018**, *10*, 7442-7450.

(36) Gao, W.; Wang, J.; Zhang, X.; Sun, L.; Chen, Y.; Zhao, Y. Electric-tunable Wettability on a Paraffin-infused Slippery Pattern Surface. *Chem. Eng. J.* **2020**, *381*, 122612.

(37) Liu, Z.; Yang, X.; Pang, G.; Zhang, F.; Han, Y.; Wang, X.; Liua, X.; Xue, L. Temperature-Based Adhesion Tuning and Superwettability Switching on Superhydrophobic Aluminum Surface for Droplet Manipulations. *Surf. Coatings Tech.* **2019**, *375*, 527–533.

(38) Chen, C.; Huang, Z.; Jiao, Y.; Shi, L.A.; Zhang, Y.: Li, J.; Li, C.; Lv, X.; Wu, S.; Hu, Y.; Zhu, W.; Wu, D.; Chu, J.; Jiang, L. In Situ Reversible Control between Sliding and Pinning for Diverse Liquids under Ultra-Low Voltage. *ACS Nano* **2019**, *13*, 5742-5752.

(39) Gulfam, R.; Zhang, P.; Meng, Z. Advanced Thermal Systems Driven by Paraffin-Based Phase Change Materials-A Review. *Appl. Energy* **2019**, *238*, 582-611.

(40) Gulfam, R.; Zhang, P. Power Generation and Longevity Improvement of Renewable Energy Systems via Slippery Surfaces–A Review. *Renew. Energy* **2019**, *143*, 922-938.

(41) Tress, M.; Karpitschka, S.; Papadopoulos, P.; Snoeijer, J.H.; Vollmer, D.; Butt, Hans-Jurgen. Shape of A Sessile Drop on A Flat Surface Covered with A Liquid Film. *Soft Matter* **2017**, *13*, 3760-3767.

(42) Gulfam, R. Synthesis, Characterization and Applications of Paraffin-Based Phase Change Materials with Enhanced Thermal Conductivity and High Energy Storage Capacity. *MS Thesis, Beihang University, Beijing, China.* **2017**.

(43) Yang, B.; Raza, A.; Bai, F.; Zhang, T.; Wang, Z. Microstructural Evolution within Mushy Zone during Paraffin's Melting and Solidification. *Int. J. Heat Mass Transfer* **2019**, *141*, 769-778.

(44) Smith, J.D.; Dhiman, R.; Anand, S.; Reza-Garduno, E.; Cohen, R.E.; Mckinleya, G.H.; Varanasi, K.K. Droplet Mobility on Lubricant-Impregnated Surfaces. *Soft Matter*, **2013**, *9*, 1772-1780.

(45) Kobald, M.; Toson, E.; Ciezki, H.; Schlechtriem, S.; Betta, S.D.; Coppola, M.; DeLuca, L. Rheological, Optical and Ballistic Investigations of Paraffin-based Fuels for Hybrid Rocket Propulsion Using a Two-Dimensional Slab-Burner. Prog. Propulsion Physics **2016**, *8*, 263-282.

(46) Piscitelli, F.; Saccone, G.; Gianvito, A.; Cosentino, G.; Mazzola, L. Microcrystalline Paraffin Wax as Fuel for Hybrid Rocket Engine. *6th European Conference for Aeronautics and Space Sciences (EUCASS)*, **2015**.

(47) Golovko, D. S.; Butt, H.-J.; Bonaccurso, E. Transition in the Evaporation Kinetics of Water Microdrops on Hydrophilic Surfaces. *Langmuir* **2009**, *25(1)*, 75-78.

(48) Orejon, D.; Sefiane, K.; Shanahan, M. E. R. Stick–Slip of Evaporating Droplets: Substrate Hydrophobicity and Nanoparticle Concentration. *Langmuir* **2011**, *27(21)*, 12834-12843.

(49) Antonini, C.; Lee, J. B.; Maitra, T.; Irvine, S.; Derome, D.; Tiwari, M.K.; Carmeliet, J.; Poulikakos, D. Unraveling Wetting Transition Through Surface Textures with X-Rays: Liquid Meniscus Penetration Phenomena. *Sci. Reports* **2014**, *4*, 4055.

(50) Xu, W.; Leeladhar, R.; Kang, Y.T.; Choi, C.-H. Evaporation Kinetics of Sessile Water Droplets on Micropillared Superhydrophobic Surfaces. *Langmuir* **2013**, *29*, 6032-6041.

(51) Erbil, H. Y.; Mchale, G.; Newton, M.I. Drop Evaporation on Solid Surfaces: Constant Contact Angle Mode. *Langmuir* **2002**, *18(7)*, 2636-2641.

(52) Shanahan, M. E. R.; Bourgès, C. Effects of Evaporation on Contact Angles on Polymer Surfaces. *Int. J. Adhesion Adhesives* **1994**, *14(3)*, 201-205.

(53) Wang, Z.; Orejon, D.; Sefiane, K.; Takata, Y. Water Vapor Uptake into Hygroscopic Lithium Bromide Desiccant Droplets: Mechanisms of Droplet Growth and Spreading. *Phys. Chem. Chem. Phys.* **2019**, *21(3)*, 1046-1058.

(53) Guan, J. H.; Wells, G. G.; Xu, B.; McHale, G.; Wood, D.; Martin, J.; Stuart-Cole, S. Evaporation of Sessile Droplets on Slippery Liquid-Infused Porous Surfaces (SLIPS). *Langmuir* **2015**, *31(43)*, 11781-11789.

(54) Wells, G. G.; Ruiz-Gutiérrez, É.; Le, L.Y.; Nourry, A.; Orme, B. V.; Pradas, M.; Ledesma-Aguilar, R. Snap Evaporation of Droplets on Smooth Topographies. *Nature Comm.* **2018**, *9(1)*, 1380.

(55) Orejon, D.; Askounis, A.; Takata, Y.; Attinger, D. Dropwise Condensation on Multiscale Bioinspired Metallic Surfaces with Nanofeatures. *ACS Appl. Mater. Interfaces* **2019**, *11*, 24735−24750.

(56) Rose, J. W.; Glicksman, L. R. Dropwise Condensation-the Distribution of Drop Sizes. *Int. J. Heat Mass Transfer* **1973**, *16(2)*, 411-425.

(57) Watanabe, N.; Aritomi, M.; Machida, A. Time-Series Characteristics and Geometric Structures of Drop-Size Distribution Density in Dropwise Condensation. *Int. J. Heat Mass Transfer* **2014**, *76*, 467-483.

(58) Anand, S.; Paxson, T.A.; Dhiman, R.; Smith, D.J.; Kripa, K.; Varanasi, K.K. Enhanced Condensation on Lubricant-Impregnated Nanotextured Surfaces. *ACS Nano* **2012**, *6(11)*, 10122-10129.

(59) Weisensee, P.B.; Wang, Y.; Qian, H.; Schultz, D.; King, W.P.; Miljkovic, N. Condensate Droplet Size Distribution on Lubricant-Infused Surfaces. *Int. J. Heat Mass Transfer* **2017**, *109*, 187-199.

(60) Rykaczewski, K.; Paxson, A.T.; Staymates, M.; Walker, M.L.; Sun, X.; Anand, S.; Srinivasan, S.; Mckinley, G.H.; Chinn, J.; Scott, J.H.J.; Varanasi, K.K. Dropwise Condensation of Low Surface Tension Fluids on Omniphobic Surfaces. *Sci. Reports* **2014**, *4*, 4158.

(61) Sett, S.; Sokalski, P.; Boyina, K.; Li, L.; Rabbi, K.F.; Auby, H.; Foulkes, T.; Mahvi, A.; Barac, G.; Bolton, L.W.; Miljkovic, N. Stable Dropwise Condensation of Ethanol and Hexane on Rationally Designed Ultrascalable Nanostructured Lubricant-Infused Surfaces. *Nano Lett*. **2019**, *19*, 8, 5287-5296.

(62) Maeda, Y.; Lv, F.; Zhang, P.; Takataa, Y.; Orejon, D. Condensate Droplet Size Distribution and Heat Transfer on Hierarchical Slippery Lubricant Infused Porous Surfaces. *Appl. Therm. Eng.* **2020**, *176*, 115386.